Contamination of frequency magnitude slope (b-value) by quarry blasts: an example for Italy

Laura Gulia[1*] and Paolo Gasperini[1,2]

[1] University of Bologna, Department of Physics and Astronomy, Bologna.

[2] Istituto Nazionale di Geofisica e Vulcanologia, Bologna, Italy

L. Gulia: Laura Gulia (laura.gulia@unibo.it)

P. Gasperini: Paolo Gasperini (paolo.gasperini@unibo.it)

[*]*corresponding author:* Laura Gulia, University of Bologna, Department of Physics and Astronomy, Viale Berti Pichat, 8 - 40127 Bologna (Italy), laura.gulia@unibo.it

The authors acknowledge there are no conflicts of interest recorded

Abstract

Artifacts often affect seismic catalogues: among them, the presence of man-made contaminations such as quarry blasts and explosions is a well-known problem. Using a contaminated dataset reduces the statistical significance of results and can lead to erroneous conclusions, thus the removal of such non-natural events should be the first step for a data analyst. Blasts misclassified as natural earthquakes, indeed, may artificially alter the seismicity rates and then the b-value of the Gutenberg and Richter relationship, an essential ingredient of several forecasting models.

At present, datasets collect several useful information beyond the parameters to locate the quakes in space and time, allowing also the users to discriminate natural and non-natural events. However, selecting them from Web Services queries is neither easy nor clear and part of such supplementary but fundamental information can be lost during downloading. As a consequence, most of statistical seismologists ignore the presence in seismic catalog of explosions and quarry blasts and assume that they were not located by seismic networks or in case they were eliminated.

We here show the example of the Italian Seismological Instrumental and Parametric Database: what happens when artificial seismicity is mixed with natural one?

Introduction

Data analysis is a fundamental part of science and statistical seismology made important steps forward both in understanding and forecasting earthquake dynamics in the last decades, also thanks to the increasing development of seismic networks and data acquisition techniques. Besides the main parameters (location, time, magnitude), indeed, each event is nowadays also characterized by several additional attributes describing the source as well as the origin of the event itself.

Although databases contain an ever-increasing number of the events' properties, some of them might be lost when data are downloaded from the websites using simplified web accesses. We here show the case of the Italian Seismological Instrumental and Parametric Database, ISIDe (ISIDe Working Group, 2007), where the event type (earthquake, quarry blast, explosion etc.) is indicated since 1 May 2012, but such info is

lost during direct downloading from the website http://terremoti.ingv.it in txt format. Indeed, the user can custom the search in terms of time, magnitude range, location (longitude, latitude and depth) but cannot discriminate the event type (http://terremoti.ingv.it/en/search), also because the presence of non-tectonic events in the database is not clearly described in the website itself. As a consequence, non-natural events such as quarry blasts, controlled, experimental and mining explosions, may be processed together with tectonic quakes.

How does such loss of info impact the statistical analysis? What happens when artificial seismicity is mixed with natural one?

The maximum magnitude of quarry and mine blasts in Europe is usually assumed to be 2.5-3.0 (Gulia, 2010; Giardini et al., 2004), which corresponds to the blast of about 100-500 kg of TNT, assuming the standard energy release of about 4 MJ per kg of TNT and the Gutenberg and Richter energy-magnitude relation. A higher threshold has been observed in US, where the magnitude of quarry and mine blasts can occasionally exceed magnitude 4 (Stump et al., 2002). Having low magnitudes, the non-natural events enrich the number of small earthquakes in a catalog, falsifying the relative portion of microseismicity respect to the higher magnitudes. This might alter the relative earthquake size distribution and then the b-value of the frequency-magnitude relationship by Gutenberg and Richter (1944). The Gutenberg and Richter relationship is a fundamental ingredient of several short-term forecasting models: among them, the Epidemic Type Aftershock Sequence (ETAS) (Ogata, 1988, 1998) that is used in Operational Earthquake Forecasting (e.g. Jordan et al., 2011), the Short-Term Earthquake Probability model (STEP; Gerstenberger et al., 2005) and the Foreshock

Traffic Light System (Gulia and Wiemer, 2019; Gulia et al., 2020). Many authors pointed out that the b-value is a proxy of the state of the stress of a region (e.g. Wyss, 1973), being inversely correlated to it and showed the b-value capability to be a "stressmeter" of the Earth's crust at different scales: from laboratory specimens (e.g., Scholz, 1968) to observations (Schorlemmer and Wiemer, 2005; Schorlemmer et al., 2005; Tormann et al., 2015; Gulia et al., 2010, 2016, 2018; Petruccelli et al., 2018, 2019a, 2019b). The b-value can have a precursory drop before the failure (Papadopoulos et al., 2010; Nanjo et al., 2012; Schurr et al., 2014; Tormann et a., 2015; Gulia et al., 2016; Gulia and Wiemer, 2019; Huang et al., 2020) suggesting that the seismicity evolution in terms of b-value should be routinely monitored. Such finding is confirmed in numerous laboratory studies, showing an increasing relative proportion of larger events as the system approaches failure (e.g. Goebel et al., 2013).

The higher b-values, resulting from an artificial enrichment of the portion of low-magnitude events in regional catalogs, can mask the spatio-temporal variations, altering the alerts and be misinterpreted as a change in the natural phenomena.

Long-term models can also be affected by falsified seismic rates and b-values: in the probabilistic seismic hazard assessment (PSHA, usually based on Cornell, 1968), the Gutenberg and Richter relationship defines event rates used to compute expected levels of ground shaking. PSHA, indeed, assumes a Poissonian distribution of seismicity and such requirement is generally satisfied by declustering the input catalog (Gardner and Knopoff, 1974, van Stiphout et al., 2010): for such reason, in the hazard assessment, rates are estimated on declustered catalogs (Field et al., 2014; Petersen et al., 2018; Wiemer et al., 2009). Mizrahi et al. (2021) show that declustering can introduce a systematic bias to the size distribution of earthquakes, potentially biasing hazard

assessment and Iervolino (2019) proposes a generalization of the hazard integral to re-introduce aftershocks in PSHA. However, at present, the seismic rates are still estimated on declustered catalogs: once the aftershocks are removed, the relative portion of quarry blasts, if present, increases as these latter usually occur almost uniformly in time, and the b-value of the grid node or zone affected by artificial events, too. As a consequence, the rates of the highest magnitudes are underestimated. Although in Italy the input dataset is usually cut at magnitude 4, in other Countries (e.g. Switzerland; Wiemer et al., 2009) the threshold magnitude cutoff is lower.

Stress-based spatiotemporal models, that describe the aftershocks productivity, can also be biased by quarry blasts: the expected rate of earthquakes in a given magnitude range (e.g., Dietrich, 1994) is indeed a function of the background seismicity.

It is important to note that high b-values can be observed in different natural settings, such as the volcanic regions (e.g., Wyss et al., 1997, 2001; Roberts et al., 2015) as well as in Enhanced Geothermal Systems during the co-injection period (Bachmann et al., 2012) and in hydrocarbon reservoirs during extraction of natural gas (Muntendam-Bos et al., 2017). Being able to discriminate between natural, induced and not-natural b-values can help seismologists to understand and interpret the physical phenomena under investigation.

For all the reasons above, non-natural events must be identified, mapped, and excluded from the catalogues before any meaningful statistical analysis can be performed. Statistical seismologists use catalogues assuming explosions have been eliminated but, as we showed before in the case of direct download from some websites, such events can erroneously be included in the catalogs.

Italy is an ideal testing region due to the simultaneous presence of a dense seismic network and several extraction sites. In 2014 the number of mining and quarrying active extraction sites in Italy was equal to 4,612 (http://www4.istat.it/) and a detailed map is available at *The Italian Institute for Environmental Protection and Research, ISPRA,* website (https://www.isprambiente.gov.it/en/istitute) but no information is given on which of them use explosives.

Explosives are the primary source of energy for rock breaking in the mining, quarrying and construction industries (Sanchidria´n et al. 2007; Hamdi et al. 2008), particularly for the building materials. Underground mines and blasting are also excavated by explosions as well as salt and coal basins are mined by blasting. Explosives are also largely employed in civil engineering (e.g. tunnel and subway) and in offshore seismic prospecting.

Wiemer and Baer (2000) proposed a purely statistical tool to identify quarry and mine blasts based on the ratio between daytime to nighttime events (from now on D/N). In the case of all-natural events, such value should be around 1 ideally or more probably slightly lower, due to the lower magnitude detection threshold in nighttime owing to the lower level of anthropic seismic noise. On the contrary, the presence of non-natural events should increase such ratio because mine blasts are usually performed during daytime.

In this work, we first show the D/N maps performed, by the tool proposed by Wiemer and Baer (2000), for two versions of ISIDe: the one downloaded directly from the Website in txt format and the one downloaded by INGV Web Services

(http://webservices.ingv.it/fdsnws/event/1/), selecting the event type *earthquake*, in the period 2005-2020. Then, by the comparison with the related b-value maps, we show the correspondence between unusually high b-values in the maps (b>1.4-1.5) to the areas with the highest D/N: the presence of non-natural events, mixed with natural ones, falsifies both the seismic rates and the b-value of the Gutenberg and Richter relationship.

Gulia (2010) mapped the daytime to nighttime ratio for the available European regional catalogs, highlighting the presence of numerous quarry blasts; among them the Italian Seismicity Catalogue (C.S.I. 1.1; Castello et al. 2006), that contains about 100.000 earthquakes during period 1981-2002. From 1 May 2012, the indication of event-types different from *earthquake* is routinely provided by the Italian Seismic Network: we thus repeat the same analysis on the dataset downloaded via Web Service, selecting only the event type *earthquake*: are all the events contained in such version, earthquakes only? Are all the quarry blasts recorded by the network, correctly identified?

Data and Method

We compute the daytime-nighttime ratio maps (Figure 1 a-d) for different time periods, on a 10-km regularly spaced grid using the events, within a 20-km radius from each node, taken from ISIDe (ISIDe Working Group, 2007). ISIDe contains the parameters of earthquake locations computed by the INGV National Seismic Network since 1985 but as input data for our estimates, we select events from 16 April 2005 (last access on 30 November 2020), when the Italian Seismic Network was reorganized and extended and

176 the quality of hypocentral locations and magnitudes was definitely improved, to 30
177 November 2020..
178 The D/N is defined as:
179
180 $$Rq = Nd\ Ln/Nn\ Ld. \quad (1)$$
181
182 where Nd is the total number of events in the daytime, Nn in the nighttime period, Ld is
183 the number of hours in the daytime period and Ln in the nighttime period. According to
184 Wiemer and Baer (2000), an indicative value for the anomalous D/N is >1.5, well
185 highlighted by the implemented color palette that, from around 1.5, abruptly changes
186 from blue-sky to pink shades. We define as *daytime* the hours from 7 a.m. to 6 p.m. and
187 *nighttime* the hours from 6 p.m. to 7 a.m. Note that according to eq. 1 the number of
188 events in each time window are normalized to the number of hours (11 for *day* -Ld- and
189 13 for *night* -Ln-).
190
191 We then establish 3 different time periods:
192 • 16 April 2005 - 30 November 2020: the whole dataset downloaded in txt format
193 at http://terremoti.ingv.it/en/search;
194 • 16 April 2005-30 April 2012, when the event-type info is not yet available:
195 natural and non-natural events are mixed together and indicated with event type
196 *earthquake*; they can be identified only by statistical analysis. Even a dataset
197 downloaded via Web Services, specifying the event type *earthquakes*, is
198 contaminated by non-natural events in the time period preceding May 2012;
199 • 1 May 2012 - 30 November 2020: when the even-type info is available. For such
200 time interval, we calculate two maps: one for the events downloaded in txt

format from http://terremoti.ingv.it/en/search and one selecting only the events identified as "earthquakes" via Web Services (http://webservices.ingv.it/fdsnws/event/1/).

We then calculate the b-value map for the two catalogs (the one containing all the events and the one contained the events classified as *earthquake* only) in the whole period 16 April 2005 – 30 November 2020 (Figure 2 a-b), using the same grid and the same radius adopted in Figure 1 a-d. The magnitude of completeness is estimated at each grid node (*Maximum Curvature*, Wiemer and Wyss, 2000) with a 0.2 correction (Woessner and Wiemer, 2005) and we require a minimum sample size of 50 events above Mc to compute the b-value by the maximum likelihood method. Note that we couldn't estimate a b-value for all the grid nodes with an already associated D/N due to the minimum number of events above Mc required for the b-value.

For some of the grid nodes with anomalous D/N, we show the histograms of the hour of the events, that represents a first and effective tool to identify the presence of quarry blasts in a catalog: quarry and mines rich regions, indeed, reveal a typical pattern, with a very large number of events during daytime hours.

Results

In all the four maps, anomalous high D/N are sparse on the whole Italian territory and most of them have been identified and described in Gulia (2010), corresponding to known excavation districts, such as Apuane-Garfagnana and Fabriano (respectively, areas D and F in Figure 1a; see Table 1 for the list of the excavation districts in Figure 1a). The user, in the case of a download in txt format at

http://terremoti.ingv.it/en/search, would unconsciously download also a big number of non-natural events, that would then be erroneously processed as earthquakes (Figure 1a).

Since the event types different from *earthquake* are specified only from 1 May 2012, even a dataset downloaded via Web Services specifying the event type as *earthquake* would be contaminated by non-natural events till such date: Figure 1b shows the D/N map from 2005 to 30 April 2012. Unluckily, copious non-natural events are inevitably downloaded from Web Services in any case also by a user who selects only the event type *earthquake*. The high contaminated regions are about the same of Figure 1a.

The last two maps (Figure 1 c-d) show and compare the D/N, in the time period staring from the event type identification (May 2012), for the two catalogs. Here also the contaminated regions are about the same of Figure 1 a-b, but often with a smaller size and value, due to the partial blasts' identification, that somewhat reduces the gap between the number of daily and nighttime events.

The similarity between these two maps (2012-2020) compared to the previous period (2005-2012, Figure 1b), indeed, points out the improved capability of the network operators to detect and identify non-natural events in some areas, however a very significant contamination still persists. Before analyzing in detail the most contaminated regions, we compare the D/N maps in Figure 1 with the two b-value maps in Figure 2 a-b, for the whole time period and for the two catalogs: most of the regions with an unusually high b-value (>1.4-1.5) and a corresponding high D/N (>1.5) are well-known active excavations districts. Furthermore, the correspondence between high D/N and high b-values is well represented in Figure 2 c-d, where we plot the D/N and the b-value for all the grid nodes of the maps: the b-values in the range that is usually observed in different natural settings (0.6-1.2/1.3) are well correlated with the typical

values of the daytime to nighttime ratio, that is around 1 and lower. On the contrary, unusually high b-values correspond mainly to the highest daytime to nighttime ratios.

In the Introduction we wonder whether all the quarry blasts recorded by the network are correctly identified: by the observation of the above maps and plots, we may already claim they are not. However, hereafter, we will list and comment in detail the regions, labeled from A to J in Figure 1a, by the analysis of some specific grid nodes with anomalous D/N and the comparison, when possible, with the corresponding b-values, for the time periods 16 April 2005 - 30 April 2012 and 1 May 2012 - 30 November 2020.

The histograms containing the hour of the day of the total number of the events for the regions A-B-C-E are shown in Figure 3, together with their seismicity maps. The relative daytime to nighttime ratios are displayed too. In these four regions, most of the events have been recorded between 10 a.m. and 3 p.m., with a minimum around the lunch break (e.g., Figure 3 c-d-k-o), as already pointed out in Gulia (2010). The spatial clusters of events locate the active quarries (Castello and Pagagnone, 2016; see also the websites https://www.regione.vda.it/territorio/territorio/attivita_estrattive/cave/cave_autorizzate_i.aspx; http://www.pianidibacino.ambienteinliguria.it/SV/03centa/varianti/DDG_2019_7664.pdf). In the regions A and B (Figure 3 a-h) the D/N of the second time period, that is when the catalog should contain only earthquakes, is even higher than in the previous one. On the contrary, the D/N in the regions C and E (Figure 3 i-p) decreases with time but remains higher than 1.5, indicating a partial identification of non-natural events; however, the three very restricted, well-defined and isolated spatial clusters in the seismicity map of the grid node in region E (Figure 3n) are the best visual example,

among the several ones we analyzed, of the highly-suspected non-natural origin of the events. In this grid node, the daytime events have been recorded mostly between 9.55 a.m. and 10 a.m. during Spring and Summer and between 10.55 a.m. and 11 a.m. during Autumn and Winter, indicating a one-hour shifted time of the blasting operations due to the daylight-saving time on Spring-Summer in Italy. Such *peculiarity* characterizes also the events in the time period following May 2012, where the quarry blasts should had been identified and classified with the correct *event type* by the network.

For these four regions, where quarries and mines are active and the natural seismicity is very low, we couldn't calculate and compare the b-values of the two time periods.
But what happen in seismically active regions with working quarries and mines? That is the case of the regions labeled as D and F in Figure 4 and G in Figure 5, that are excavation districts, also affected by natural seismicity.

In Figure 4 we show a seismically active area in Northern Tuscany (area D in Figure 1a): the Apuane-Garfagnana district, that is a well-known excavation district since the age of ancient Romans: the white marble, also known as "white gold", that artists like Michelangelo Buonarroti and Antonio Canova transformed in world heritage masterpieces, was mined here. In the first time period, from April 2005 till the end of April 2012, the events in this small area are spatially clustered (D2) and the histogram of the hour of the events (Figure 4b) shows the typical pattern of quarry rich area: the events are concentrated between 9 a.m. and 11 a.m. In the following time period (from 1 May 2012 to 30 November 2020), the events are still spatially clustered (Figure 4f) but towards the North (D1) and the histogram of the hour of the events (Figure 4g)

300 shows now the typical pattern of a slightly contaminated area: the nighttime hours have
301 the highest peaks but there are still peaks around 10 a.m. and 3 p.m. That is due to the
302 simultaneous identification of most of blasts (The D/N of D2 passes from 40 to 1.8, for
303 example; Figure 4 d and i) and to a seismic sequence with a maximum M_L of 4.8 that hit
304 the region on January 2013 (D1): its aftershocks increases the number of events in the
305 grid nodes, that passed from about 30 events per year to 90 whilst the overall b-value
306 decreases from 1.5 (almost all blasts) to 1.1 (blasts and aftershocks; Figure 4e). It is
307 important to note that, in the epicentral area of the M_L 4.8, the D/N remains below 1,
308 even if a very small contamination is clear (hours 11 a.m. and 3 p.m., Figure 4h), in fully
309 agreement with Wiemer and Baer (2000): the detection threshold is generally lower
310 during the day due to the ambient noise and, as a consequence, regions not containing
311 quarries generally show a decrease in the number of events detected during the day and
312 an increase during the night. Thus, we should expect a D/N lower than 1 in the case of
313 natural seismicity and this grid node is a perfect illustration. The same grid node
314 illustrates also the example of non-natural events, in D2.
315 In this region, the b-value results from the mixing of natural and not-natural events:
316 there has been a strong improvement with time and most of blasts are now correctly
317 identified by the network, even if a further effort is required to identify and remove all
318 of them.
319
320 In Figure 4 j-r, we show the case of a grid node in a seismically active area with only low
321 magnitude events (area F in Figure 1a; the Cingoli district, Marche), that is another well-
322 known and wide extraction district of the Country, already described in Gulia (2010). In
323 the seismicity maps (Figure 4 j and n), the events are spatially clustered in few main
324 areas: we here choose two of them, named F1 and F2, to compare the evolution with

time of a seismically active area (F1) with an extraction one (F2). Before May 2012, only 3 events have been recorded in F1 and more than 80% of the events in the whole grid node occurred during daily hours: the D/N of the node is 5.5 (Figure 4k); after such date, the D/N passes to 0.8, showing a small blast contamination (Figure 4o). The D/N of the natural seismicity in F1 is always below 1, while the D/N in F2 decreases from 70 to about 6: as already shown in the previous case, most of blasts are nowadays identified by the network, but several ones still remain.

The overall b-value of the events in the grid node, before May 2012, is 1.4 (Figure 4r): a very high value respect to the one expected from this area, considering its prevalent style-of-faulting (Gulia and Wiemer, 2010). After such date, the b-value decreases to 1.2, possibly due to the increment of natural seismicity and the contemporary partial identification of non-natural events. As for the grid node in region D, the overall b-value results from the mixture of natural and non-natural events.

Figure 5 illustrates two interesting case studies: the first one is about a grid node in the region labeled as G in Figure 1a, Central Italy. Natural and non-natural seismicity are mixed together, as revealed by the histograms of the hour of the events of two small spatial clusters (G1 and G2): before May 2012, 349 events out of 354, in G1, are daytime events and the relative b-value (1.9 in Figure 5e) is unusually high, more than twice that typical, according to Gulia and Wiemer (2010), for the region. The G1 excavation area has been successfully identified after 2012, indeed ISIDe, in the following period, contains only 4 events, 2 during daytime and 2 during nighttime. Few blasts still remain also in the adjacent areas G2; however, this area has been successfully located by the network operators and most of non-natural events identified. The overall b-value decreases to 1.1.

As well as for the previous case, in the grid node in area H (Figure 5 j-r) most of blasts have been successfully identified: the D/N of the whole area passes from 5 to 1 and the b-value decreases from 1.2 (resulting from many blasts and few natural events) to 0.9 (few blasts Figure 5r).

The last two case studies, shown in Figure 6 (areas labeled as I and J in Figure 1a), exhibit a similar evolution in time. Most of the seismicity before May 2012 is composed by non-natural events: the D/N are, respectively, 2.6 and 43 (Figure 6 b and k) and the b-values 1.7 and 2.2 (Figure 6 e and r), among the highest values in the whole Country. After May 2012, both D/N and b-value decreases, possibly due to the correct but still partial identification of non-natural events.

Finally, since quarry blasts are performed during the day, the nighttime events should be all tectonic and scale with a lower b-value respect to the daytime events. We then divided the events according to the hour of the day for the above grid nodes with low-magnitude events only and show the comparison of the frequency magnitude distributions for the two periods (Figure 7). The theoretical expected behavior is fully confirmed for all the five nodes: the nighttime b-value are all well below the daytime ones, in some cases less than the half.

Discussion and Conclusion

Every day, beyond tectonic events, seismic networks detect several non-natural quakes: among them, quarry and mine blasts are the most numerous anthropogenic recorded

events. Often, such events are not identified and thus collected together with tectonic events.

Having low magnitudes, the artificial events enrich the number of small earthquakes in a catalog, contaminating the natural signals and seismicity datasets adulterating the relative portion of microseismicity respect to the higher magnitudes. The resulting seismic rate changes and the relative earthquake size distribution, or b-value of the Gutenberg and Richter relationship (1944), are falsified.

The natural signal is then contaminated, impacting many short-term forecasting models, such as ETAS (Ogata, 1988, 1998) or the FTLS (Gulia and Wiemer, 2019), where seismic rates and b-value, both inferred from the Gutenberg and Richter relationship, are a basic ingredient.

Long-term analysis, such as PSHA, can be also impacted by non-natural events: quarry blasts, if present, increase the b-value of the grid node or zone affected by artificial events, resulting in an underestimation of the highest-magnitude rates.

In this work we show the example of the Italian Seismological Instrumental and Parametric Database, where the *event types* of the non-natural events are available since 1 May 2012 only. In the *Custom Search* page (http://terremoti.ingv.it/en/search), the user can set the starting and the end date, the Magnitude as well as the Latitude/Longitude and the Depth ranges but the Event Type is not mentioned. Being the event type not available among the *Custom Search* options in ISIDe, the user downloads also non-natural events, not being conscious of this.

Other online available catalogs, for example The ANSS Comprehensive Earthquake Catalog (ComCat; https://earthquake.usgs.gov/earthquakes/search/) by U.S. Geological Survey (USGS), allows the user to set also the Event Type among the *Advanced Options*. The Event Type option for ISIDe can be set only when retrieving data via Web Services.

We download and compare two versions of ISIDe: one downloaded at http://terremoti.ingv.it/en/search and one via Web Services, specifying the Event Type *earthquake*: are all the non-natural events correctly recognized? If not, how much non-natural events, misclassified as earthquakes, do impact the b-value?

As a first test, we spatially map the ratio of daytime to nighttime events (D/N), proposed by Wiemer and Baer (2000) to investigate the presence of quarry blasts, for different time-intervals of the two catalogs, showing that:

- in the whole period (16 April 2005 – 30 November 2020) the dataset downloaded at http://terremoti.ingv.it/en/search in txt format is heavily contaminated by quarry blasts in the whole Italian territory (Figure 1a);
- the period 16 April 2005 – 30 April 2012, where the event type is always indicated as *earthquake* and thus the events are common to both catalogs, shows an even wider contamination that can be detected only by statistical analysis (Figure 1b);
- the following time period, that is 1 May 2005 – 30 November 2020, is still highly contaminated by non-natural events in both catalogs (Figure 1 c-d); however, in the known extraction districts, there is a general improvement for the catalog

downloaded via Web Services. Some areas where extractions started after 2012 (e.g. area B, Figure 3b) seem to be unknown.

We then spatially map the b-value for the two catalogs by using the same grid and radius already adopted for the D/N maps (Figure 2 a-b): since we required a minimum number of events above Mc to calculate the b-value, not all the grid nodes with a D/N have a corresponding b-value. The regions with unusually high b-values (>1.4-1.5) well correspond to the regions with high D/N in Figure 1. To further highlight the correlation between high b-value and high D/N, we plot the two values for the same grid nodes (Figure 2 c-d), confirming the correspondence.

Some of the grid nodes with anomalous D/N have been analysed in detail: for such areas, we show the seismicity maps, the histograms of the hour of the events (Figures 3 to 6) and, when possible, the frequency magnitude distributions before and after 1 May 2012. There has been a general improvement with time and several quarry blasts are now correctly identified by the network's operators, however many ones still remain, affecting the b-value estimations and increasing the portion of low-magnitude events.

The seismicity of the grid node in Figure 4a-i offers an incisive and clear example of artificial b-value temporal fluctuations due to non-tectonic events: it is an excavation area hit by a Ml 4.8 in 2013. If we compare the frequency magnitude distributions of the two periods (Figure 4e), we note an apparent 27% b-value decrease (from 1.5 to 1.1): according to several forecasting models and to evidence from laboratory specimens, such decrease should suggest a change in the physical condition of the region, resulting somewhat in an alert for an impending strong earthquake.

Finally, since quarry blasts are performed during the day, we expect that the all the nighttime events are natural quakes: we compare, in Figure 7, the frequency magnitude distributions of daytime and nighttime events for some of the previous analyzed grid nodes with no events with magnitude greater than 3.5: all the daytime b-value are higher than the nighttime ones.

Our analysis reveals the presence of numerous quarry blasts in the Italian Seismological Instrumental and Parametric Database, ISIDe (ISIDe Working Group, 2007) in the period 16 April 2005 – 30 April 2012, misclassified as earthquakes. After 1 May 2012, there is a general improvement in identifying the event type. However, many quarry blasts are still not correctly classified and such improvement is lost when the user downloads the event list at http://terremoti.ingv.it/en/search in txt format.

Data and Resources

The Italian Seismological Instrumental and Parametric Database, ISIDe (ISIDe Working Group, 2007), is available at http://terremoti.ingv.it/en/search and from INGV Web Services for full download (webservices.ingv.it/fdsnws/event/1/).

Both figures and calculations were performed by MATLAB, available at www.mathworks.com/products/matlab.

Declaration of Competing Interests

The authors declare no competing interests

Acknowledgments

The authors thank the editors, Allison Bent and Anastasia Pratt, and two anonymous reviewers for helping in improving and clarifying the article. The authors also thank Gianfranco Vannucci and Stefan Wiemer for their comments on the preliminary version of the manuscript, and Barbara Lolli and Daniele Randazzo for having provided the catalog file from WebServices with the indication of event types. This study was supported by the Real-time earthquake rIsk reduction for a reSilient Europe (RISE) project, funded by the European Union's Horizon 2020 research and innovation program under Grant Agreement Number 821115 and partially funded by the Pianeta Dinamico-Working Earth INGV-MIUR project.

References

Bachmann. C., S. Wiemer, B.P. Goertz-Allmann, and J. Woessner (2012). Influence of pore-pressure on the event-size distribution of induced earthquakes, *Geophys. Res. Lett.*, **39**(9), L09302, doi:10.1029/2012GL051480

Castello, B., G. Selvaggi, C. Chiarabba, and A. Amato (2006). CSI catalogo della sismicità italiana 1981–2002, versione 1.1, Ist. Naz. di Geofis. E Vulcanol., Rome. (Available at http://www.ingv.it/CSI/)

Castello C., and Pagagnone, M. (2016). Minerali, miniere e cave del Parco Naturale Mont Avic (Comuni di Champdepraz e Champorcher - Valle d'Aosta - Alpi Occidentali), REV. Valdôtaine Hist. Nat., **70**, 7-56. http://www.sfv.it/public/uploads/Revue/2016%2070/Revue2016_1_Castello%20&%20Paganone.pdf

499

500 Cornell, C.A. (1968). Engineering seismic risk analysis, *Bull. Seism. Soc. Am.*, **58**, 1583–
501 1606.

502

503 Dieterich, J. H. (1994). A constitutive law for rate of earthquake production and its
504 application to earthquake clustering, J*. Geophys. Res*., **99**, 2601–2618.

505

506 Field, E. H., R.J. Arrowsmith, G.P. Biasi, P. Bird, T.E. Dawson, K.R. Felzer, *et al.* (2014).
507 Uniform California earthquake rupture forecast, version 3 (UCERF3)—The time-
508 independent model, *Bull. Seismol. Soc. Am.*, **104,** no. 3**,** 1122-1180.

509

510 Gardner, J. K., and L. Knopoff (1974). Is the sequence of earthquake in Southern
511 California, with aftershocks removed, Poissonian? *Bull. Seismol. Soc. Am.*, **66**, 1271–
512 1302.

513

514 Giardini D., S. Wiemer, D. Fäh, and D. Deichmann (2004). Seismic hazard assessment of
515 Switzerland, Report, Swiss Seismological Service, ETH Zurich, 88 pp

516

517 Gerstenberger, M. C., S. Wiemer, L. M. Jones, and P.A. Reasenberg (2005). Real-time
518 forecasts of tomorrow's earthquakes in California, *Nature*, **435**, no. 7040, 328–331.
519 https://doi.org/10.1038/nature03622

520

521 Goebel, T. H. W., D. Schorlemmer, T. W. Becker, G. Dresen, and C. G. Sammis (2013).

522 Acoustic emissions document stress changes over many seismic cycles in stick-slip
523 experiments, *Geophys. Res. Lett.* **40**, 2049–2054, doi: 10.1002/grl.50507.
524
525 Gulia, L., A.P. Rinaldi, T. Tormann, G. Vannucci, B. Enescu, and S. Wiemer (2018). The
526 effect of a mainshock on the size distribution of the aftershocks, *Geophys Res Lett*, **45**.
527 doi: 10.1029/2018GL080619
528
529 Gulia, L., S. Wiemer, and G. Vannucci (2020). Pseudoprospective Evaluation of the
530 Foreshock Traffic-Light System in Ridgecrest and Implications for Aftershock Hazard
531 Assessment, *Seismol. Res. Lett.* **91**, no. 5, 2828–2842, doi: 10.1785/0220190307.
532
533 Gulia L. and S. Wiemer (2019). Real-time discrimination of earthquake foreshocks and
534 aftershocks. *Nature,* **574**, 193-199.
535
536 Gulia, L., T. Tormann, S. Wiemer, M. Herrmann, and S. Seif (2016). Short-term
537 probabilistic earthquake risk assessment considering time dependent b values, *Geophys.*
538 *Res. Lett*. **43**, 1100–1108, doi: 10.1002/2015GL066686.
539
540 Gulia, L., and S. Wiemer (2010). The influence of tectonic regimes on the earthquake size
541 distribution: A case study for Italy, *Geophys Res Lett*, **37**, L10305. doi:
542 10.1029/2010GL043066
543
544 Gulia, L. (2010). Detection of quarry and mine blast contamination in European regional
545 catalogues, *Nat. Hazards*, **53**, 229-249, doi: 10.1007/s11069-009-9426-8.
546

547 Gulia, L., S. Wiemer and D. Schorlemmer (2010). Asperity-based earthquake likelihood
548 models for Italy, *Ann. Geophys*, **53**, no. 3. doi: 10.4401/ag-4843
549
550 Gutenberg, B., and C. F. Richter (1944). Frequency of earthquakes in California, *Bull.*
551 *Seismol. Soc. Am.* **34**, 185–188.
552
553 Hamdi E, N. Bouden Romdhane, J. du Mouza, and J.M. Le Cleac'h (2008). Fragmentation
554 energy in rock blasting, *Geotech Geol Eng* , **26**, 133–146

555 Huang H., L. Meng, R. Burgmann, W. Wang, and K. Wang, (2020). Spatio-temporal
556 foreshock evolution of the 2019 M 6.4 and M 7.1 Ridgecrest, California earthquakes,
557 *Earth Planet. Sci. Lett.* **551**, 116582, ISSN 0012-821X, doi: 10.1016/j.epsl.2020.116582.

558 Iervolino, I. (2019). Generalized earthquake counting processes for sequence-based
559 hazard, *Bull. Seismol. Soc. Am*. **109**, no. 4, 1435–1450.
560
561 ISIDe Working Group (2007). Italian Seismological Instrumental and Parametric
562 Database (ISIDe), Istituto Nazionale di Geofisica e Vulcanologia (INGV).
563 https://doi.org/10.13127/ISIDE
564
565 Jordan, T.H., Y. Chen, R. Madariaga, i. Main, W. Marzocchi, G. Papadopulos, G. Sobolev, K.
566 Yamaoka, and J. Zschau (2011). Operational earthquake forecasting: state of knowledge
567 and guidelines for implementation, final report of the international commission on
568 earthquake forecasting for civil protection, *Ann. Geophys*., **54**, no. 4, 315–391.
569

570 Mizrahi L., S. Nandan and S. Wiemer (2021), The Effect of Declustering on the Size
571 Distribution of Mainshocks, *Seismol. Res. Lett.*, doi: 10.1785/ 0220200231.

572

573 Muntendam-Bos, A., J. Roset and H. De Waal (2017). The effect of imposed production
574 measures on gas extraction induced seismic risk, *Netherlands J. Geoscience*, **96**, no. 5,
575 S271-S278, doi: 10.1017/njg.2017.29

576

577 Nanjo, K. Z., N. Hirata, K. Obara, and K. Kasahara (2012), Decade-scale decrease in b
578 value prior to the M9-class 2011 Tohoku and 2004 Sumatra quakes, *Geophys. Res. Lett.,*
579 **39**, L20304, doi:10.1029/2012GL052997.

580

581 Ogata, Y. (1988). Statistical models for earthquake occurrences and residual analysis for
582 point processes, *J. Am. Stat. Assoc*., **83**, no. 401, 9–27.

583

584 Ogata, Y. (1998). Space-time point-process models for earthquake occurrences, *Ann.*
585 *Inst. Stat. Math.,* **50**, no. 2, 379–402, doi:10.1023/A:1003403601725.

586

587 Papadopoulos, G. A., M. Charalampakis, A. Fokaefs, and G. Minadakis (2010). Strong
588 foreshock signal preceding the L'Aquila (Italy) earthquake (Mw 6.3) of 6 April 2009,
589 *Nat. Hazards Earth Syst.* Sci., **10**, 19–24.

590

591 Petersen, M. D., C.S. Mueller, M.P. Moschetti, S.M. Hoover, K.S. Rukstales, D.E. McNamara,
592 ... and A.L. Llenos (2018). 2018 one-year seismic hazard forecast for the central and

593 eastern United States from induced and natural earthquakes, *Seismol. Res. Lett.*, **89**, no.
594 3, 1049-1061.
595
596 Petruccelli, A., P. Gasperini, T. Tormann, D. Schorlemmer, A. P. Rinaldi, G. Vannucci, and
597 S.Wiemer (2019a). Simultaneous dependence of the earthquake-size distribution on
598 faulting style and depth, *Geophys. Res. Lett*. **46**, no. 20, 11044–11053, doi:
599 10.1029/2019GL083997.
600
601 Petruccelli, A., D. Schorlemmer, T. Tormann, A. P. Rinaldi, S. Wiemer, P. Gasperini, and G.
602 Vannucci (2019b). The influence of faulting style on the size-distribution of global
603 earthquakes, *Earth Planet. Sci. Lett*. **527,** doi: 10.1016/j.epsl.2019.115791.
604
605 Petruccelli A., G. Vannucci, B. Lolli and P. Gasperini (2018). *Harmonic fluctuation of the*
606 *slope of the frequency - magnitude distribution (b-value) as a function of the angle of rake*,
607 *Bull. Seismol. Soc. Am*., **108**, 1864-1876, doi: 10.1785/0120170328.
608
609 Roberts, N. S., A.F. Bell, and I.G. Main (2015). Are volcanic seismic b-values high, and if
610 so when? *J. Volc. Geoth. Res*., **308**, 127-141, ISSN 0377-0273, doi:
611 10.1016/j.jvolgeores.2015.10.021.
612
613 Sanchidria´n JA, P. Segarra, L.M. Lo´pez, (2007). Energy components in rock blasting, *Int*
614 *J. Rock Mech. Min. Sci.* **44**, 130–147
615

616 Scholz, C. H. (1968). The frequency-magnitude relation of microfracturing in rock and
617 its relation to earthquakes, *Bull. Seismol. Soc. Am*. **58**, 399–415.
618
619 Schorlemmer, D., and S. Wiemer (2005). Microseismicity data forecast rupture area,
620 *Nature*, 434, 1086, doi:10.1038/4341086a.
621
622 Schorlemmer, D., S. Wiemer, and M. Wyss (2005). Variations in earthquake-size
623 distribution across different stress regimes, *Nature,* **437**, no. 7058, 539–542,
624 doi:10.1038/nature04094.
625
626 Schurr, B., G. Asch, S. Hainzl, *et al.* (2014). Gradual unlocking of plate boundary
627 controlled initiation of the 2014 Iquique earthquake, *Nature*, **512**, 299–302,
628 doi:10.1038/nature13681.
629
630 Stump, B. W., M.A.H. Hedlin D.C. Pearson, and V. Hsu (2002). Characterization of mining
631 explosions at regional distances: Implications with the International Monitoring System,
632 *Rev. Geophys.* **40 ,** no. 4, 2–21, doi: 10.1029/1998RG000048.
633
634 Tormann, T., B. Enescu, J. Woessner, and S. Wiemer (2015). Randomness of megathrust
635 earthquakes implied by rapid stress recovery after the Japan earthquake, *Nat. Geosci*., **8**,
636 152–158, doi:10.1038/ngeo2343.
637
638 van Stiphout, T., S. Wiemer, and W. Marzocchi (2010). Are short-term evacuations
639 warranted? Case of the 2009 L'Aquila earthquake, *Geophys. Res. Lett*., **37**, L06306,
640 doi:10.1029/2009GL042352.

Wiemer, S., G. Giardini, D. Fäh, N. Deichmann, and S. Sellami, (2009). Probabilistic seismic hazard assessment of Switzerland: best estimates and uncertainties, *J. Seism.*, **13**, no. 4, 449.

Wiemer, S., and M. Wyss (2000). Minimum Magnitude of completeness in earthquake catalogs: Examples from Alaska, the western US and Japan, *Bull. Seismol. Soc. Am.*, **90**, 859–869.

Wiemer, S. and M. Baer (2000). Mapping and removing quarry blast events from seismicity catalogs, *Bull. Seism. Soc. Am.* **90**, no. 2, 525–530

Woessner, J. and S. Wiemer (2005). Assessing the quality of earthquake catalogues: Estimating the magnitude of completeness and its uncertainty, *Bull. Seismol. Soc. Am*. **95**, 684–698.

Wyss, M. (1973). Towards a Physical Understanding of the Earthquake Frequency Distribution, *Geophys. J. Int.*, **31**, no. 4, 341–359, doi: 0.1111/j.1365-246X.1973.tb06506.x

Wyss, M., K. Shimazaki, and S. Wiemer (1997). Mapping active magma chambers by *b* values beneath the off-Ito volcano, Japan, *J. Geophys. Res.*, **102**, B9, 20,413-20,422, doi: 10.1029/97JB01074

665 Wyss, M., F. Klein, K. Nagamine, and S. Wiemer (2001). Anomalously high b-values in the
666 South Flank of Kilauea volcano, Hawaii: evidence for the distribution of magma below
667 Kilauea's East rift zone, J. Volc. Geoth. Res., **106,** no. 1–2, 23-37, ISSN 0377-0273, doi:
668 10.1016/S0377-0273(00)00263-8.

669

670 **Authors'adress**

671 Laura Gulia, University of Bologna, Department of Physics and Astronomy, Viale Berti
672 Pichat, 8 - 40127 Bologna (Italy)

673

674 Paolo Gasperini, University of Bologna, Department of Physics and Astronomy, Viale
675 Berti Pichat, 8 - 40127 Bologna (Italy)

676 **Table**

Letter	Excavation District	Material
A	Albiano - Trento	Porphyry
B	Issogne-Gressoney	Green marble, Limestone, Slate
C	Savona	Limestone and Quartzite
D	Apuane-Garfagnana	White, Red and black marble
E	Maremma	Limestone
F	Cingoli-Marche	Limestone
G	Riofreddo	Limestone and Basalt
H	Gargano	Marble and Limestone
I	Altamura-Matera	Limestone and Marble
J	Siracusa	Porphyry and Basalt

Table 1 – List of the excavation districts labeled in Figure 1 with the letters A-J and the extracted material.

Figure captions

Figure 1 A-D. Maps of the daytime to night-time ratio (D/N): a) for the time interval 2005-2020 and for the whole dataset downloaded in txt format at http://terremoti.ingv.it/en/search. The letters A-J correspond to the excavation districts listed in Table 1. b) for the time interval 16 April 2005 - 30 April 2012, where the events are classified with event type *earthquake*; c) for the time interval 1 May 2012 – 30 November 2020, for all the events downloaded in txt format at http://terremoti.ingv.it/en/search; d) for the time interval 1 May 2012 - 30 November 2020, for all the events downloaded via Web Services selecting the event type *earthquake* only. The maps are computed on a 10-km regularly spaced grid using the events within a 20-km radius from each node.

Figure 2 A-D. a-b) Maps of the b-value for the time interval 16 April 2005 - 30 November 2020, computed on a 10-km regularly spaced grid using the events within a 20-km radius from each node for a) the whole dataset downloaded in txt format at http://terremoti.ingv.it/en/search and b) the whole dataset downloaded via Web Services selecting the event type *earthquake* only. c-d) plot of the D/N against the b-value for all the grid nodes adopted in the previous maps for c) the whole dataset downloaded in txt format at http://terremoti.ingv.it/en/search and d) the whole dataset downloaded via Web Services selecting the event type *earthquake*.

Figure 3 A-P. Spatial and statistical analysis of four grid nodes n the areas labeled as A-B-C and E in Figure 1a. a-b) Seismicity maps and histograms of the hours of the events (c-d) for a grid in area A for, respectively, the events downloaded at http://terremoti.ingv.it/en/search in the period 16 April 2005 - 30 April 2012 and for the events downloaded via Web Services selecting the event type *earthquake* from 1 May 2012 - 30 November 2020. e-f) Seismicity maps and histograms of the hours of the events (g-h) for a grid in area B for, respectively, the events downloaded at http://terremoti.ingv.it/en/search in the period 16 April 2005 - 30 April 2012 and for the events downloaded via Web Services selecting the event type *earthquake* from 1 May 2012 - 30 November 2020. i-j) Seismicity maps and histograms of the hours of the events (k-l) for a grid in area C for, respectively, the events downloaded at http://terremoti.ingv.it/en/search in the period 16 April 2005 - 30 April 2012 and for the events downloaded via Web Services selecting the event type *earthquake* from 1 May 2012 - 30 November 2020. m-n) Seismicity maps and histograms of the hours of the events (o-p) for a grid in area E for, respectively, the events downloaded at http://terremoti.ingv.it/en/search in the period 16 April 2005 - 30 April 2012 and for the events downloaded via Web Services selecting the event type *earthquake* from 1 May 2012 - 30 November 2020.

Figure 4 A-R. Spatial and statistical analysis of two grid nodes n the areas labeled as D and F. Grid node in area D in the time period 16 April 2005 - 30 April 2012: a) seismicity map with two spatial clusters, D1 and D2, circled in black; histogram of the hour of

events and relative D/N for b) all the events in the grid node, c) all the events in the D1 spatial cluster and d) all the events in the D2 spatial cluster. Grid node in area D in the time period 1 May 2012 - 30 November 2020: f) seismicity map with two spatial clusters, D1 and D2, circled in black; histogram of the hour of events and relative D/N for g) all the events in the grid node, h) all the events in the D1 spatial cluster and i) all the events in the D2 spatial cluster. e) frequency magnitude distributions for all the events in the grid node D from 16 April 2005 to 30 April 2012 (blue circles) and from 1 May 2012 to 30 November 2020, red asterisks.

Grid node in area F in the time period 16 April 2005 - 30 April 2012: j) seismicity map with two spatial clusters, F1 and F2, circled in black; histogram of the hour of events and relative D/N for k) all the events in the grid node, j) all the events in the F1 spatial cluster and m) all the events in the F2 spatial cluster. Grid node in area F in the time period 1 May 2012 - 30 November 2020: n) seismicity map with two spatial clusters, F1 and F2, circled in black; histogram of the hour of events and relative D/N for o) all the events in the grid node, p) all the events in the F1 spatial cluster and q) all the events in the F2 spatial cluster. r) frequency magnitude distributions for all the events in the grid node F from 16 April 2005 to 30 April 2012 (blue circles) and from 1 May 2012 to 30 November 2020, red asterisks.

Figure 5 A-R. Spatial and statistical analysis of two grid nodes n the areas labeled as G and H. Grid node in area G in the time period 16 April 2005 - 30 April 2012: a) seismicity map with two spatial clusters, G1 and G2, circled in black; histogram of the hour of events and relative D/N for b) all the events in the grid node, c) all the events in

745 the G1 spatial cluster and d) all the events in the G2 spatial cluster. Grid node in area G
746 in the time period 1 May 2012 - 30 November 2020: f) seismicity map with two spatial
747 clusters, G1 and G2, circled in black; histogram of the hour of events and relative D/N
748 for g) all the events in the grid node, h) all the events in the G1 spatial cluster and i) all
749 the events in the G2 spatial cluster. e) frequency magnitude distributions for all the
750 events in the grid node G from 16 April 2005 to 30 April 2012 (blue circles) and from 1
751 May 2012 to 30 November 2020, red asterisks.

752 Grid node in area H in the time period 16 April 2005 - 30 April 2012: j) seismicity map
753 with two spatial clusters, H1 and H2, circled in black; histogram of the hour of events
754 and relative D/N for k) all the events in the grid node, j) all the events in the H1 spatial
755 cluster and m) all the events in the H2 spatial cluster. Grid node in area H in the time
756 period 1 May 2012 - 30 November 2020: n) seismicity map with two spatial clusters, H1
757 and H2, circled in black; histogram of the hour of events and relative D/N for o) all the
758 events in the grid node, p) all the events in the H1 spatial cluster and q) all the events in
759 the H2 spatial cluster. r) frequency magnitude distributions for all the events in the grid
760 node H from 16 April 2005 to 30 April 2012 (blue circles) and from 1 May 2012 to 30
761 November 2020, red asterisks.

762

763 ***Figure 6 A-R***. Spatial and statistical analysis of two grid nodes n the areas labeled as I
764 and J. Grid node in area I in the time period 16 April 2005 - 30 April 2012: a) seismicity
765 map with two spatial clusters, I1 and I2, circled in black; histogram of the hour of events
766 and relative D/N for b) all the events in the grid node, c) all the events in the I1 spatial
767 cluster and d) all the events in the I2 spatial cluster. Grid node in area I in the time

768 period 1 May 2012 - 30 November 2020: e) seismicity map with two spatial clusters, I1
769 and I2, circled in black; histogram of the hour of events and relative D/N for g) all the
770 events in the grid node, h) all the events in the I1 spatial cluster and i) all the events in
771 the I2 spatial cluster. f) frequency magnitude distributions for all the events in the grid
772 node I from 16 April 2005 to 30 April 2012 (blue circles) and from 1 May 2012 to 30
773 November 2020, red asterisks.

774 Grid node in area J in the time period 16 April 2005 - 30 April 2012: j) seismicity map
775 with two spatial clusters, J1 and J2, circled in black; histogram of the hour of events and
776 relative D/N for k) all the events in the grid node, j) all the events in the J1 spatial
777 cluster and m) all the events in the J2 spatial cluster. Grid node in area J in the time
778 period 1 May 2012 - 30 November 2020: n) seismicity map with two spatial clusters, J1
779 and J2, circled in black; histogram of the hour of events and relative D/N for o) all the
780 events in the grid node, p) all the events in the J1 spatial cluster and q) all the events in
781 the J2 spatial cluster. r) frequency magnitude distributions for all the events in the grid
782 node J from 16 April 2005 to 30 April 2012 (blue circles) and from 1 May 2012 to 30
783 November 2020, red asterisks.

784

785 ***Figure 7*.** Comparison of the frequency magnitude distributions for the five grid nodes
786 in Figures 3 to 6 with low-magnitude events only (B, C, G, I and J) for all the daytime
787 (black circles) and nighttime (grey squares) events for the dataset downloaded via Web
788 Services (event type *earthquake*) from16 April 2005 to 30 November 2020.

789

790

791

792 **Figures**

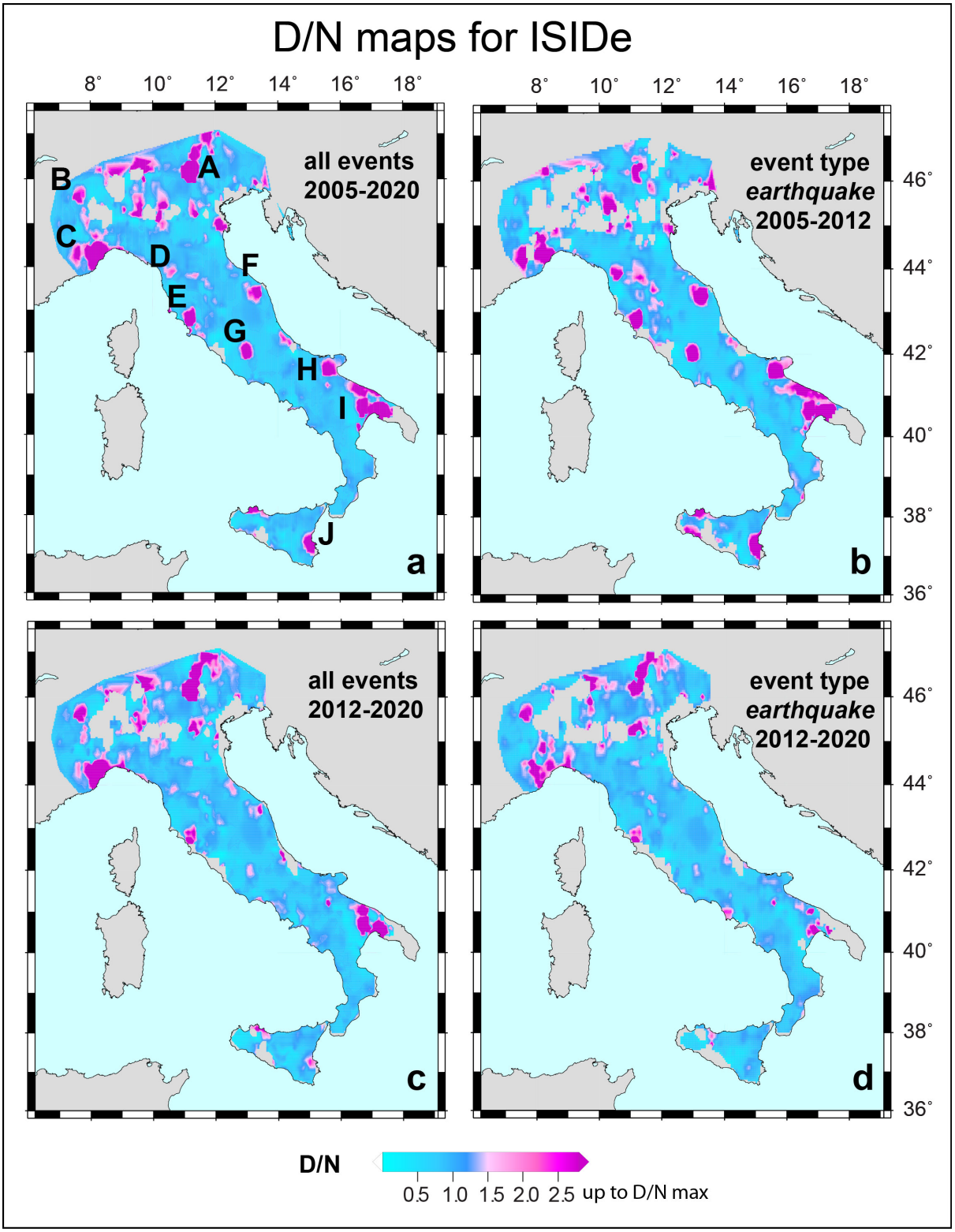

793

794 ***Figure 1 A-D.*** Maps of the daytime to night-time ratio (D/N): a) for the time interval
795 2005-2020 and for the whole dataset downloaded in txt format at

http://terremoti.ingv.it/en/search. The letters A-J correspond to the excavation districts listed in Table 1. b) for the time interval 16 April 2005 - 30 April 2012, where the events are classified with event type *earthquake*; c) for the time interval 1 May 2012 – 30 November 2020, for all the events downloaded in txt format at http://terremoti.ingv.it/en/search; d) for the time interval 1 May 2012 - 30 November 2020, for all the events downloaded via Web Services selecting the event type *earthquake* only. The maps are computed on a 10-km regularly spaced grid using the events within a 20-km radius from each node.

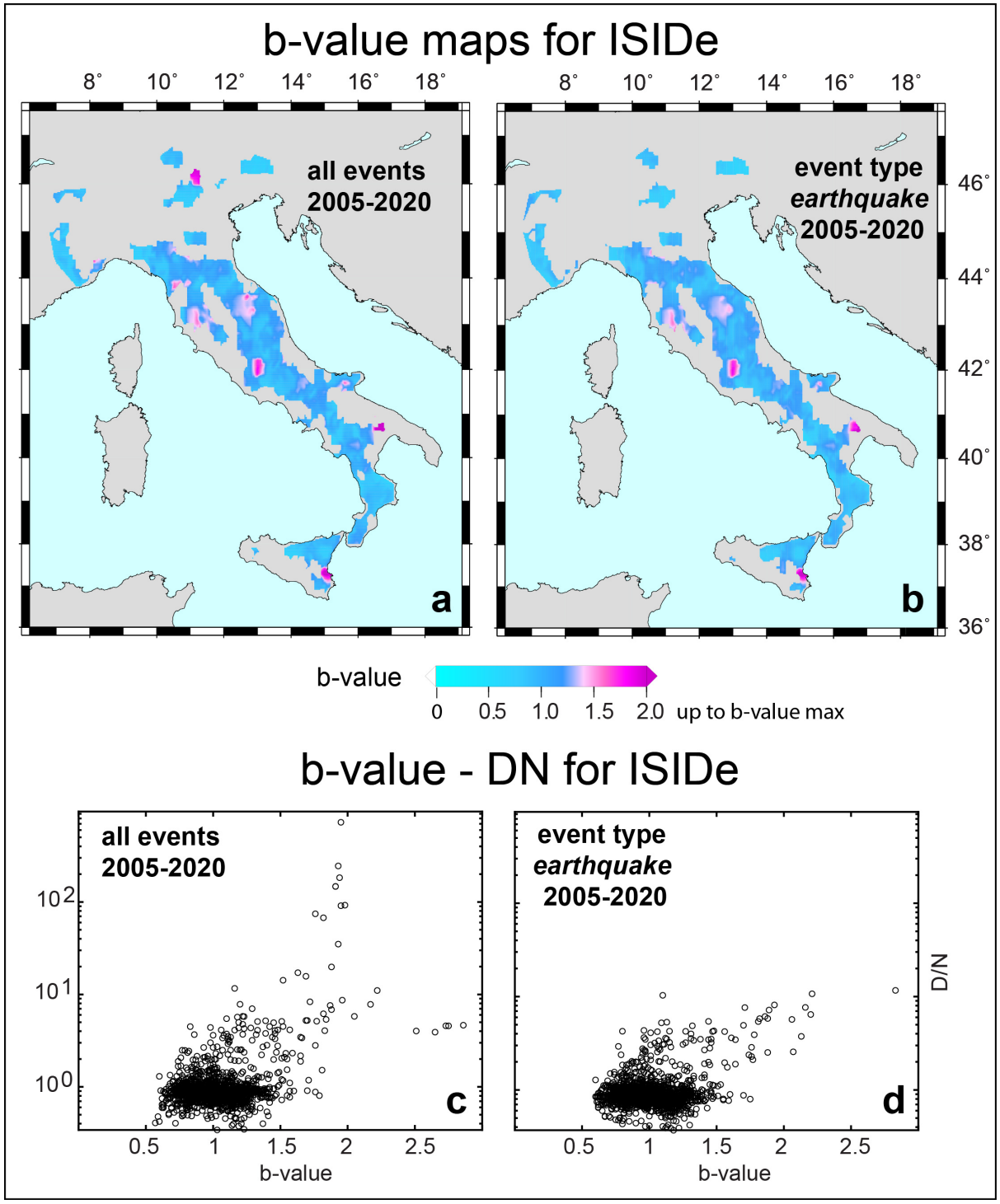

805

806

807

808 *Figure 2 A-D.* a-b) Maps of the b-value for the time interval 16 April 2005 - 30

809 November 2020, computed on a 10-km regularly spaced grid using the events within a

810 20-km radius from each node for a) the whole dataset downloaded in txt format at

811 http://terremoti.ingv.it/en/search and b) the whole dataset downloaded via Web
812 Services selecting the event type *earthquake* only. c-d) plot of the D/N against the b-
813 value for all the grid nodes adopted in the previous maps for c) the whole dataset
814 downloaded in txt format at http://terremoti.ingv.it/en/search and d) the whole
815 dataset downloaded via Web Services selecting the event type *earthquake*.

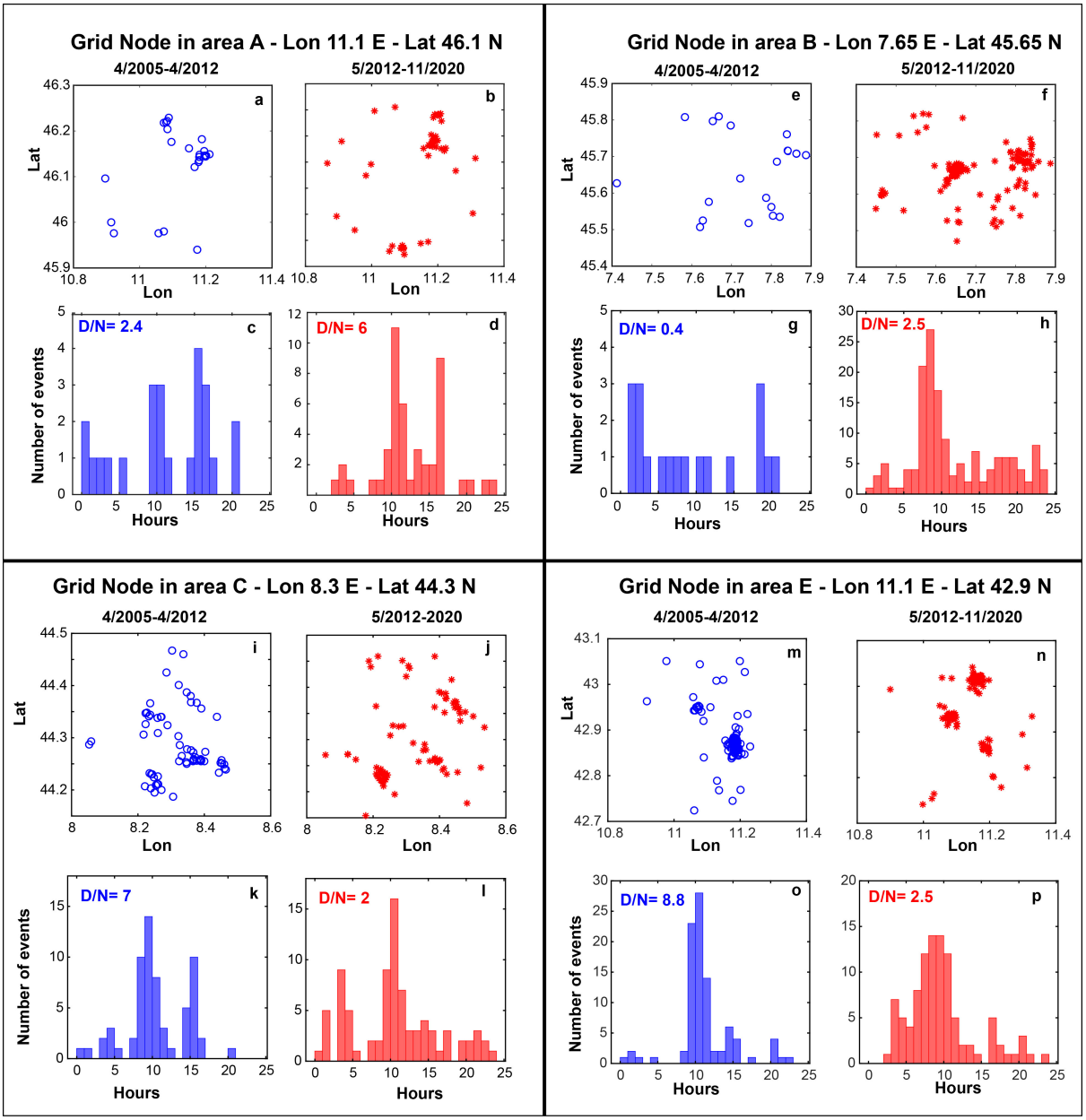

816

817 ***Figure 3 A-P***. Spatial and statistical analysis of four grid nodes in the areas labeled as A-
818 B-C and E in Figure 1a. a-b) Seismicity maps and histograms of the hours of the events
819 (c-d) for a grid in area A for, respectively, the events downloaded at
820 http://terremoti.ingv.it/en/search in the period 16 April 2005 - 30 April 2012 and for
821 the events downloaded via Web Services selecting the event type *earthquake* from 1
822 May 2012 - 30 November 2020. e-f) Seismicity maps and histograms of the hours of the
823 events (g-h) for a grid in area B for, respectively, the events downloaded at

http://terremoti.ingv.it/en/search in the period 16 April 2005 - 30 April 2012 and for the events downloaded via Web Services selecting the event type *earthquake* from 1 May 2012 - 30 November 2020. i-j) Seismicity maps and histograms of the hours of the events (k-l) for a grid in area C for, respectively, the events downloaded at http://terremoti.ingv.it/en/search in the period 16 April 2005 - 30 April 2012 and for the events downloaded via Web Services selecting the event type *earthquake* from 1 May 2012 - 30 November 2020. m-n) Seismicity maps and histograms of the hours of the events (o-p) for a grid in area E for, respectively, the events downloaded at http://terremoti.ingv.it/en/search in the period 16 April 2005 - 30 April 2012 and for the events downloaded via Web Services selecting the event type *earthquake* from 1 May 2012 - 30 November 2020.

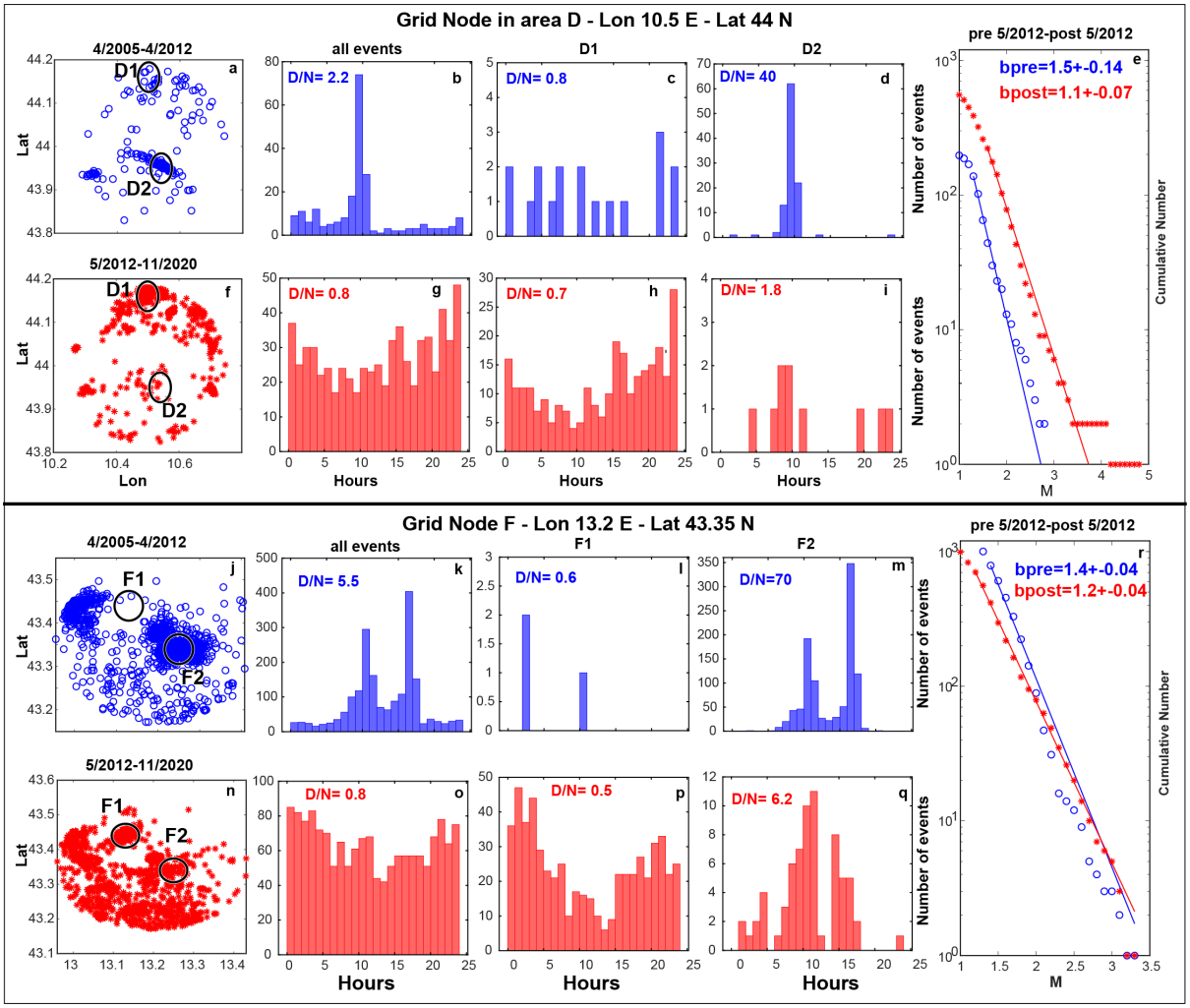

836

837 ***Figure 4 A-R***. Spatial and statistical analysis of two grid nodes in the areas labeled as D
838 and F. Grid node in area D in the time period 16 April 2005 - 30 April 2012: a) seismicity
839 map with two spatial clusters, D1 and D2, circled in black; histogram of the hour of
840 events and relative D/N for b) all the events in the grid node, c) all the events in the D1
841 spatial cluster and d) all the events in the D2 spatial cluster. Grid node in area D in the
842 time period 1 May 2012 - 30 November 2020: f) seismicity map with two spatial
843 clusters, D1 and D2, circled in black; histogram of the hour of events and relative D/N
844 for g) all the events in the grid node, h) all the events in the D1 spatial cluster and i) all
845 the events in the D2 spatial cluster. e) frequency magnitude distributions for all the

events in the grid node D from 16 April 2005 to 30 April 2012 (blue circles) and from 1 May 2012 to 30 November 2020, red asterisks.

Grid node in area F in the time period 16 April 2005 - 30 April 2012: j) seismicity map with two spatial clusters, F1 and F2, circled in black; histogram of the hour of events and relative D/N for k) all the events in the grid node, j) all the events in the F1 spatial cluster and m) all the events in the F2 spatial cluster. Grid node in area F in the time period 1 May 2012 - 30 November 2020: n) seismicity map with two spatial clusters, F1 and F2, circled in black; histogram of the hour of events and relative D/N for o) all the events in the grid node, p) all the events in the F1 spatial cluster and q) all the events in the F2 spatial cluster. r) frequency magnitude distributions for all the events in the grid node F from 16 April 2005 to 30 April 2012 (blue circles) and from 1 May 2012 to 30 November 2020, red asterisks.

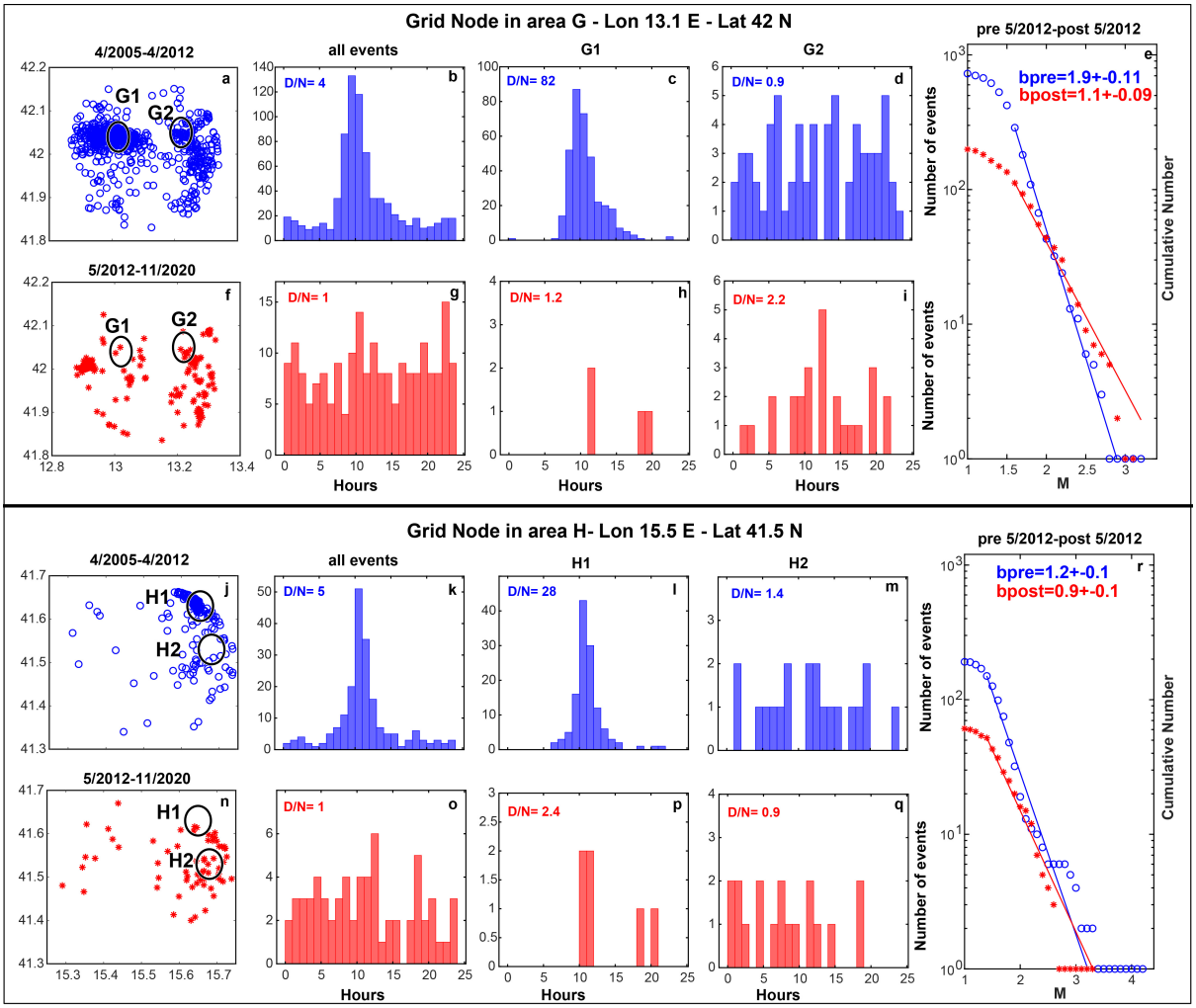

859

860 ***Figure 5 A-R***. Spatial and statistical analysis of two grid nodes n the areas labeled as G
861 and H. Grid node in area G in the time period 16 April 2005 - 30 April 2012: a)
862 seismicity map with two spatial clusters, G1 and G2, circled in black; histogram of the
863 hour of events and relative D/N for b) all the events in the grid node, c) all the events in
864 the G1 spatial cluster and d) all the events in the G2 spatial cluster. Grid node in area G
865 in the time period 1 May 2012 - 30 November 2020: f) seismicity map with two spatial
866 clusters, G1 and G2, circled in black; histogram of the hour of events and relative D/N
867 for g) all the events in the grid node, h) all the events in the G1 spatial cluster and i) all
868 the events in the G2 spatial cluster. e) frequency magnitude distributions for all the

events in the grid node G from 16 April 2005 to 30 April 2012 (blue circles) and from 1 May 2012 to 30 November 2020, red asterisks.

Grid node in area H in the time period 16 April 2005 - 30 April 2012: j) seismicity map with two spatial clusters, H1 and H2, circled in black; histogram of the hour of events and relative D/N for k) all the events in the grid node, j) all the events in the H1 spatial cluster and m) all the events in the H2 spatial cluster. Grid node in area H in the time period 1 May 2012 - 30 November 2020: n) seismicity map with two spatial clusters, H1 and H2, circled in black; histogram of the hour of events and relative D/N for o) all the events in the grid node, p) all the events in the H1 spatial cluster and q) all the events in the H2 spatial cluster. r) frequency magnitude distributions for all the events in the grid node H from 16 April 2005 to 30 April 2012 (blue circles) and from 1 May 2012 to 30 November 2020, red asterisks.

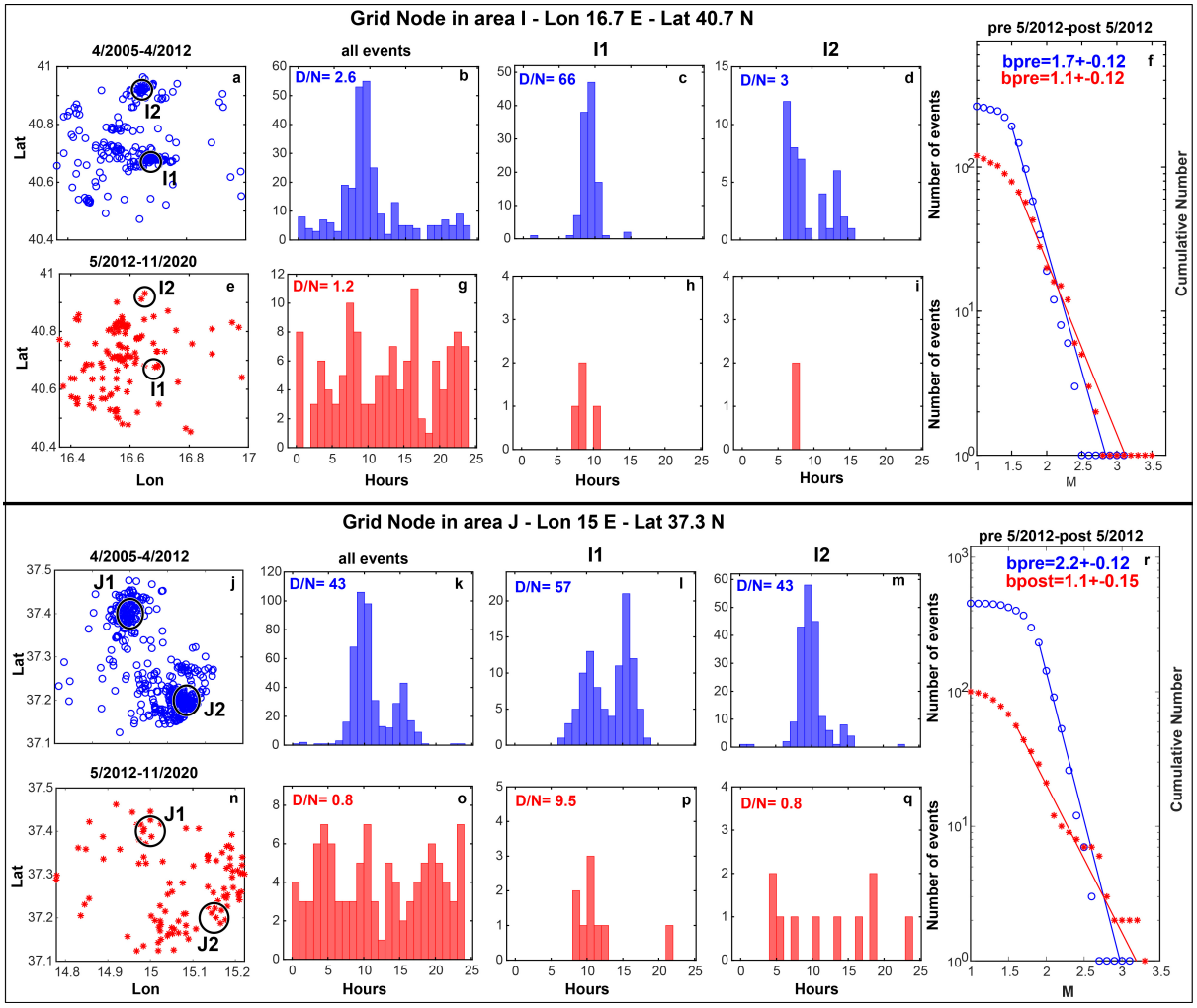

882

883 ***Figure 6 A-R***. Spatial and statistical analysis of two grid nodes n the areas labeled as I
884 and J. Grid node in area I in the time period 16 April 2005 - 30 April 2012: a) seismicity
885 map with two spatial clusters, I1 and I2, circled in black; histogram of the hour of events
886 and relative D/N for b) all the events in the grid node, c) all the events in the I1 spatial
887 cluster and d) all the events in the I2 spatial cluster. Grid node in area I in the time
888 period 1 May 2012 - 30 November 2020: e) seismicity map with two spatial clusters, I1
889 and I2, circled in black; histogram of the hour of events and relative D/N for g) all the
890 events in the grid node, h) all the events in the I1 spatial cluster and i) all the events in
891 the I2 spatial cluster. f) frequency magnitude distributions for all the events in the grid

node I from 16 April 2005 to 30 April 2012 (blue circles) and from 1 May 2012 to 30 November 2020, red asterisks.

Grid node in area J in the time period 16 April 2005 - 30 April 2012: j) seismicity map with two spatial clusters, J1 and J2, circled in black; histogram of the hour of events and relative D/N for k) all the events in the grid node, j) all the events in the J1 spatial cluster and m) all the events in the J2 spatial cluster. Grid node in area J in the time period 1 May 2012 - 30 November 2020: n) seismicity map with two spatial clusters, J1 and J2, circled in black; histogram of the hour of events and relative D/N for o) all the events in the grid node, p) all the events in the J1 spatial cluster and q) all the events in the J2 spatial cluster. r) frequency magnitude distributions for all the events in the grid node J from 16 April 2005 to 30 April 2012 (blue circles) and from 1 May 2012 to 30 November 2020, red asterisks.

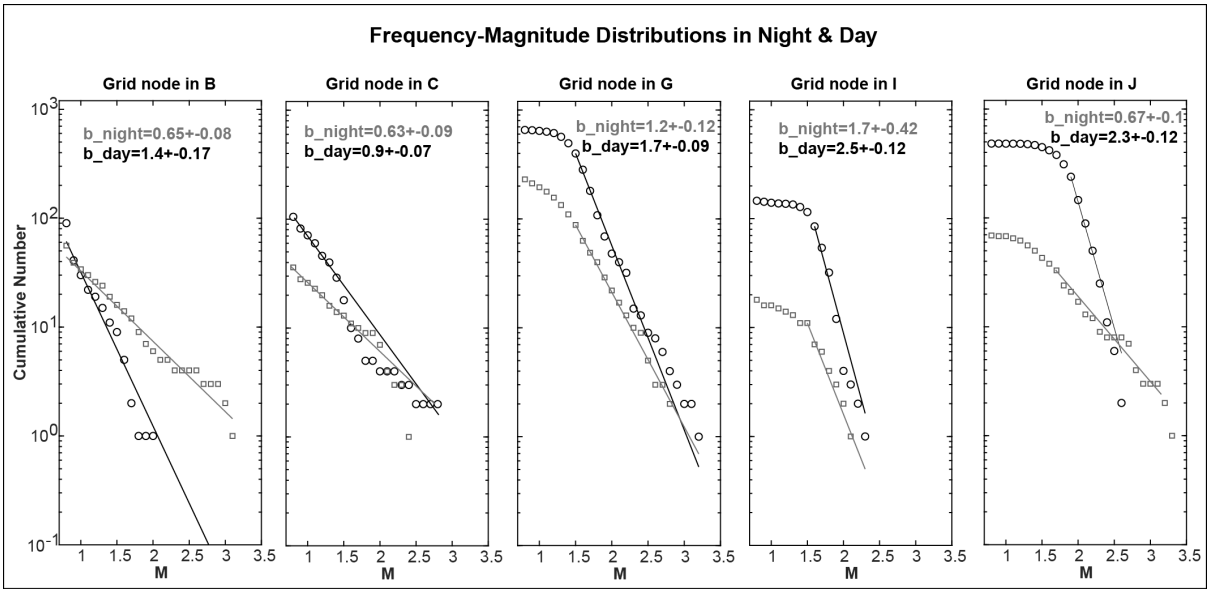

***Figure 7*.** Comparison of the frequency magnitude distributions for the five grid nodes in Figures 3 to 6 with low-magnitude events only (B, C, G, I and J) for all the daytime (black circles) and nighttime (grey squares) events for the dataset downloaded via Web Services (event type *earthquake*) from16 April 2005 to 30 November 2020.